

Second generation of vortex-antivortex states in mesoscopic superconductors: stabilization by artificial pinning

R. Geurts, M. V. Milošević, and F. M. Peeters*

Departement Fysica, Universiteit Antwerpen, Groenenborgerlaan 171, B-2020 Antwerpen, Belgium

(Dated: October 29, 2018)

Antagonistic symmetries of superconducting polygons and their induced multi-vortex states in a homogeneous magnetic field may lead to appearance of *antivortices* in the vicinity of the superconducting/normal state boundary (where mesoscopic confinement is particularly strong). Resulting vortex-antivortex (V-Av) molecules match the sample symmetry, but are extremely sensitive to defects and fluctuations and remain undetected experimentally. Here we show that V-Av states can re-appear *deep in the superconducting state* due to an array of perforations in a polygonal setting, surrounding a central hole. Such states are no longer caused by the symmetry of the sample but rather by pinning itself, which prevents the vortex-antivortex annihilation. As a result, even *micron-size, clearly spaced V-Av molecules* can be stabilized in large mesoscopic samples.

PACS numbers: 74.78.Na, 74.25.Dw, 74.25.Qt

Vortices in small superconducting elements have been the focus of scientific research ever since it was shown that a strongly confined superconducting condensate shows enhanced critical properties [1, 2]. Usually individual vortices pierce the sample in the direction of applied magnetic field, minimizing the energy of the stray magnetic field, as well as their mutual interaction. Such formed vortex clusters (called ‘multi-vortex’ [3]) tend to mimic the symmetry of the sample, due to the repulsion with the surrounding screening (Meissner) currents. In samples of the order of the coherence length ξ and/or penetration depth λ , the edge currents may even compress the vortex lines into a single bundle, often referred to as a ‘giant-vortex’ [3, 4]. However, in addition to these simple arguments, the effects of lateral confinement in mesoscopic elements can have more elaborate manifestations. One such is the appearance of *vortex-antivortex* molecules, of exact the same symmetry as the host sample.

Almost a decade since the original prediction of Chibotaru *et al.* [5] the symmetry-induced antivortex remains one of the most exciting phenomena in vortex matter in submicron superconductors. The stability of an antivortex in *opposite* magnetic field is still puzzling, and not yet verified experimentally. Latter is not surprising, taking into account that predicted vortex-antivortex molecules are very small in size ($\sim \xi$, somewhat larger in type-I samples [6]) and extremely sensitive to defects [7]. Actually, in most instances, they are simply unstable [8, 9].

In last several years, two methods were proposed to improve the stability and the observability of the vortex-antivortex states in mesoscopic polygons. In one, the magnetic field profile was altered by a magnetic dot placed on top of the superconductor [10]. The bipolar field of the added magnet favors the antivortex underneath, and repels vortices further apart. However, this method: (i) interferes with the key concept of an antivortex in opposite, unipolar field, (ii) makes the structure

more complicated, three-dimensional, and inaccessible for scanning probe techniques, and (iii) poses difficulties for any magnetic (magnetic-force, Hall-probe) measurements. Instead, we recently proposed the structural engineering of the sample itself, by strategically placed holes in the sample, mimicking the sample symmetry and the expected symmetry of the vortex-antivortex state [11]. In such realization each hole hosts (pins) one vortex, where the pinning force is effectively stronger than the vortex-antivortex attraction. As a consequence, vortices remain in the holes even when placed at further distances from the antivortex, and the whole molecule can be made significantly larger.

In this paper, we realized that not only vortices can be pinned in the latter concept, but an antivortex as well. We therefore introduced an additional, central hole in the sample, in which the antivortex can reside. Intuitively, this facilitates the quantization of negative stray flux between the vortices in a cluster, and leads to a more

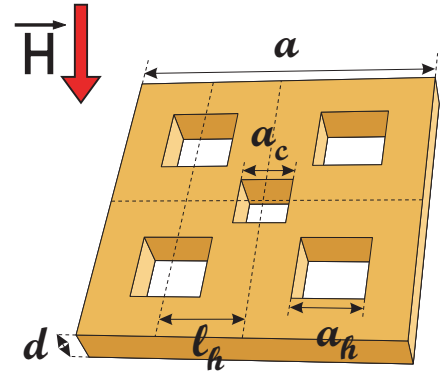


FIG. 1: A schematic drawing of a polygonal mesoscopic superconductor (side a , thickness d) with corresponding arrangement of perforations (spacing l_h , characteristic size of each hole a_h and of the central hole a_c) in a perpendicular magnetic field H .

stable antivortex. Vortices and antivortices in holes are just quantized magnetic field, screening prevents their annihilation, and the fact that they have no core reduces their attractive interaction. As will be shown, this indeed leads to an enhanced stabilization of the vortex-antivortex molecule, even deep into the superconducting state, but with significantly altered overall properties. Although this generally applies to any polygonal setting of the holes and various shapes of the sample [12], in what follows we show the proof of principle for a square superconducting geometry, as shown in Fig. 1.

For the purpose of this study, we use the mean-field, Ginzburg-Landau (GL) theory, and solve numerically the set of GL equations

$$(-i\nabla - \vec{A})^2\psi - (1 - T - |\psi|^2)\psi = 0, \quad (1)$$

$$-\kappa^2\Delta\vec{A} = \vec{j}_s = \Re\left[\psi\left(i\nabla - \vec{A}\right)\psi^*\right] \quad (2)$$

already established as a prime tool for theoretical description of mesoscopic superconductors [3]. All variables in Eqs. (1,2) are dimensionless and expressed in temperature independent units (assuming $\sim (1 - T)^{-1/2}$ dependence of characteristic length scales in the system, coherence length ξ , and penetration depth λ). $\kappa = \lambda/\xi$ is the so-called GL parameter, and describes the ability of the sample to screen the applied magnetic field. Temperature is scaled to T_c , magnetic field to $H_{c2}(0)$, vector potential to $H_{c2}(0)\xi(0)$ and the order parameter ψ to $\psi(0) = \sqrt{\alpha(0)/\beta}$. The Gibbs free energy density \mathcal{F} , in units of $\mathcal{F}(T=0, H=0) = H_c(0)^2/8\pi$ is calculated from

$$\mathcal{F} = \frac{1}{V} \int \left[\left| (-i\nabla - \vec{A})\psi \right|^2 - (1 - T - \frac{1}{2}|\psi|^2)|\psi|^2 \right] \quad (3)$$

$$+ \kappa^2(\nabla \times \vec{A} - \vec{H})^2 \Big] dV, \quad (4)$$

for each of the stable superconducting states found during the simulation. The full simulation region, used for the calculation of the magnetic response of the sample, was a square with 128 grid points in each direction. The number of grid points *inside* the sample was kept at 64×64 .

In Fig. 2 we show the free energy of vortex states with vorticities from $L = 0$ to $L = 6$ as a function of the applied magnetic flux $\Phi = a^2H$. The simulation is performed by sweeping the magnetic field up and down, and then back-tracking of all found vortex states so that their complete stability range is obtained. In addition, we performed the calculation starting from different initial conditions, some of which included reasonable guesses of possible vortex configurations. Fig. 2 summarizes all the found stable states, but we may not rule out the possibility of some more complex, higher energy, vortex states. For this simulation a square of size $20\xi(0) \times 20\xi(0)$ was used with holes of size $3.5\xi(0) \times 3.5\xi(0)$, four of which are horizontally and vertically displaced by $5\xi(0)$ from the center of the sample. Temperature was fixed at $0.3T_c$

(corresponding to Al samples below 400 mK [13]) and an extreme type-II behavior was assumed, typical for thin samples ($\kappa = \infty$). The combinatorial number of possible vortex configurations for given vorticity is quite high, and many of them are indeed found stable due to both the large size of the sample and that of the central hole. Starting from zero field, the Meissner state, $L = 0$, is the lowest energy state in the flux band of $\Delta\Phi = 1.85\Phi_0$, which is larger than a flux quantum, but significantly smaller than in non-perforated mesoscopic samples [9]. The reason is that the first vortex penetrates easier, and is more stable in the present system due to the central hole (central $L = 1$ is in the ground state in $\Delta\Phi = 1.92\Phi_0$). States with an off-center vortex have mostly higher energy, smaller stability range, and are fourfold degenerate (which makes them interesting for logic applications [14]). $L = 2$ shows the *broken symmetry* in the ground state, as two vortices reside in the central and corner hole, but their ground-state flux-band is only $\Delta\Phi = 0.17\Phi_0$. Similarly, the broken symmetry $L = 3$ state with all vortices in the corners is the ground state in a short interval of $\Delta\Phi = 0.11\Phi_0$. Just like in the superconducting square with 2×2 holes [15], $L = 4$ vortices reside in the corners and show enhanced stability in the ground state ($\Delta\Phi = 1.95\Phi_0$). However, the most dominant state in Fig. 2 is the $L = 5$ one, where all holes are occupied by a single vortex ($\Delta\Phi = 3.63\Phi_0$). Therefore, while for the square with an 2×2 holes high symmetry states as $L = 2$ and $L = 4$ were pronouncedly low-energy states, we notice that in the present system the states which have a vortex in the central hole, and are fourfold symmetric dominate the ground state, i.e. $L = 1$ and $L = 5$. Note that the $L = 4$ state is still very comfortable with the fourfold symmetry although it does not have a central vortex, but e.g. $L = 3$ with a central vortex is not in the ground state because it does not obey the symmetry of the sample. Because of their very low energy, $L = 1, 4, 5$ states overshadow other states like the $L = 2$ and $L = 3$. The $L = 3$ state has several allotropes, i.e. it can have vortices across the sample diagonal, one vortex in the center and two on the side, or all three out of the center. Only one configuration can satisfy the fourfold symmetry of the sample and that is the $L = 4 - 1$ state, with four vortices in corner holes and an *antivortex* in the center. This vortex-antivortex (V-Av) state is indeed found stable in our system, with relatively high energy, but still lower than most higher vorticity states (which suggests that it can be experimentally realized in decreasing magnetic field).

The physical origin of this V-Av state is however different from the V-Av state found in Refs. [5, 6, 7, 11] where the V-Av molecules appear due to the imposed symmetry of the sample. In Ref. [11], the added holes only reinforce the symmetry argument and do not cause *per se* the V-Av state. In the rest of the paper, we will refer to this state as the symmetry induced V-Av in contrast

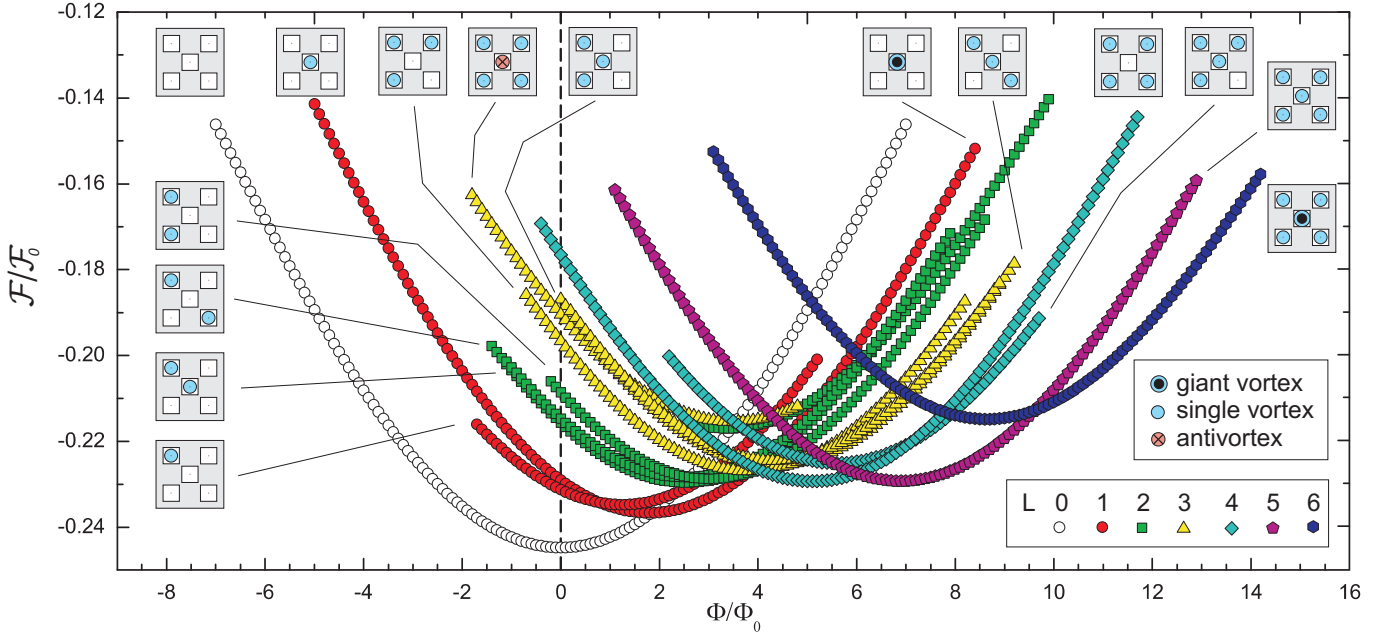


FIG. 2: The Gibbs free energy spectrum, showing the energy levels and stability of different vortex states as a function of applied magnetic field at $T = 0.3T_c$. Insets cartoon the vortex arrangement for selected states.

to the newly found V-Av state which is *fully stabilized by pinning* of all vortices and the antivortex. In Fig. 3 we show the $\Phi - T$ phase diagram for both versions of the $L = 3$ vortex-antivortex state (for taken parameters $a = 20\xi(0)$, $a_h = 3\xi(0)$, $l_h = 4\xi(0)$, $a_c = 1.5\xi(0)$, see Fig. 1). We observed two fully independent islands in the $\Phi - T$ phase space corresponding to the two manifestations of the V-Av state. The symmetry-induced one

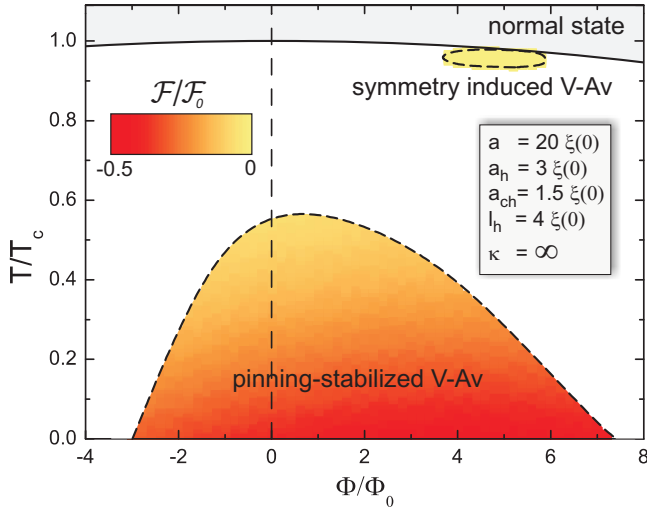


FIG. 3: The superconducting state in the $\Phi - T$ diagram (solid line shows the superconducting/normal state boundary) comprising the areas of stability of the $L = 3$ vortex-antivortex molecules, both pinning- and symmetry-induced ones. Color coding shows the energy of those vortex states.

is situated in the high temperature regime, where confinement imposed by the sample boundaries is effectively very large. It should be noted here that the ΔT stability range for the symmetry-induced V-Av state is on average just 1% larger than in the case of 2×2 holes [11] (since the order parameter inside the molecule is in any case severely suppressed). At lower temperatures, the GL equations are strongly non-linear and symmetry arguments cannot account for the nucleation of the V-Av state. Nevertheless, a second generation V-Av state does stabilize, thanks to the large spacing between the holes (preventing vortex-antivortex annihilation) and the large size of the sample (diminishing the effect of encircling screening currents). The pinning-stabilized V-Av state: 1) occupies far larger $\Phi - T$ area compared to the symmetry induced one, a wide region of $\approx 10\Phi_0$ and $\approx 0.6T_c$, and 2) it is found stable even *in negative applied field*, where central antivortex is a natural state and vortices are subjected to an increasing expulsion pressure. In principle, several vortex states are found stable at negative fields in Fig. 2, which is a manifestation of the flux-trapping effect [16]. However, out of all $L = 3$ states, $L = 4 - 1$ shows maximal resilience to negative flux.

To emphasize again, the size of the sample is playing a crucial role for the V-Av state. While the symmetry-induced V-Av exists only for small samples [compared to the coherence length $\xi(T)$] the pinning-stabilized V-Av requires a large sample. This is illustrated in Fig. 4(a) for a square with five holes. When the sample is larger, the flux stability region of the pinning stabilized V-Av state becomes larger as well. This we can attribute to

the weakened influence of the Meissner current on the inside vortices because of the larger distance. One also notices the extremely large flux interval (from $-7.5\Phi_0$ to $17\Phi_0$) for stability of the $L = 3$ pinning-stabilized V-Av state. However, penetration field for new vortices *must decrease* for larger samples (see e.g. [17] for the case of large BiSCCO disks). It is already known that magnetic field higher than H_{c1} is needed for penetration of vortices into mesoscopic superconductors, but this factor decreases to unity in bulk systems. Nevertheless, latter factor decreases with size of the sample much slower than the square power increase of the area of the sample. As a consequence, the threshold flux for penetration of new vortices in our sample *increases* as a function of $a/\xi(0)$. We also observed the changing curvature of the latter dependence (at $a/\xi(0) \approx 25$); from the calculation of threshold magnetic field, we found that samples

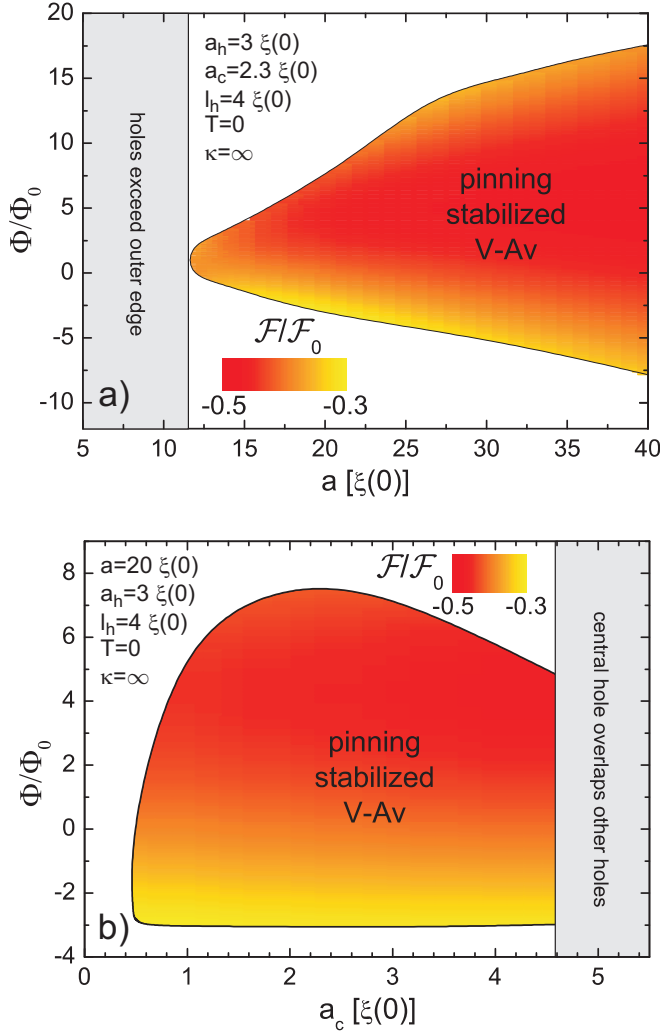


FIG. 4: The stability diagram vs. applied field (i.e. magnetic flux) for the pinning-induced vortex-antivortex state, (a) as a function of the sample size for a fixed temperature, and (b) as a function of the size of the central hole.

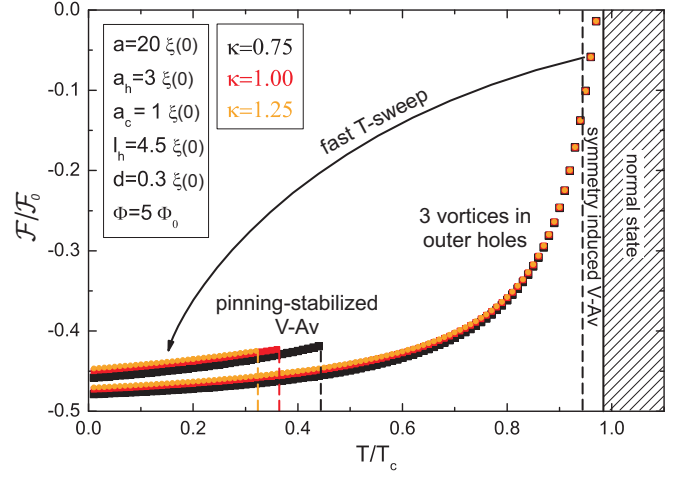


FIG. 5: The energy of V-Av molecules as a function of temperature, for different values of the Ginzburg-Landau parameter κ . In numerical simulations, an abrupt cooling enables direct transition between two kinds of V-Av states.

with size of $10\text{-}25\xi(0)$ exhibit almost identical demagnetization effects i.e. similar vortex penetration field which then gradually decreases for sizes above $25\xi(0)$.

The size of the central hole is equally important as the sample size, as it relates to the ability of V-Av pair to annihilate. Consequently, this second generation V-Av state *cannot be stabilized* in the absence of the central hole [see Fig. 4(b)]. The effect of decreasing the central hole size is also indicated in Fig. 4(b) - the upper boundary of the flux stability interval is decreasing, due to facilitated V-Av annihilation (at high fields, vortices are pushed towards the center of the sample), while the lower boundary is in fact *not influenced* by the size of the central hole. Note that lower boundary lies in the negative field region, where vortices have expulsion tendency, and pinning of any strength stabilizes the central antivortex with ease.

The latter stability of the pinned V-Av state in the negative field forms a base for the realization of this state in experiment. Namely, abrupt increase of the magnetic field from a low negative value (that stabilizes one antivortex in the sample) to a large positive one (allowing for penetration of multiple vortices in outer holes) may result in the desired V-Av state at low temperatures. Alternatively, following the results of Fig. 3, one can think of an abrupt temperature decrease. We performed a corresponding simulation, where we started from the symmetry-induced V-Av state (which is the ground state for $L = 3$ at temperatures near T_c) and then applied a steep temperature decrease. Without taking into account the experimentally relevant temperature gradient over time, the simulations were always able to land into the pinning-stabilized V-Av state at low temperatures. This is illustrated in Fig. 5 where also the influence of κ is depicted. Stronger screening of the magnetic field

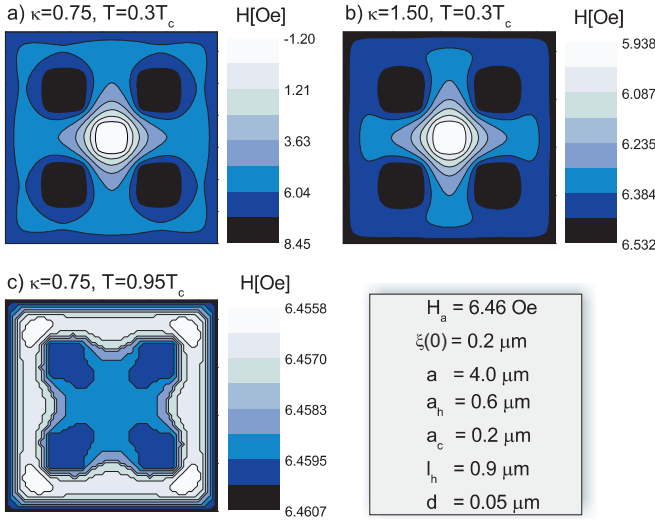


FIG. 6: Calculated magnetic field profiles in the sample: (a,b) for the pinning-stabilized V-Av state and two values of κ , and (c) the corresponding profile for the symmetry-induced V-Av state.

into the holes (i.e. lower κ) enhances the pinning, and consequently favors the V-Av state of second generation, *in contrast* to the symmetry-induced V-Av which is disfavored by low values of κ due to the effective attraction of vortices into a single bundle (see Ref. [11]).

Although quite difficult to realize (never being the ground-state of the system), the second generation V-Av state is much more suitable for direct experimental visualization than its symmetry-induced ancestor. Firstly, samples can be made larger, and spacing between vortices and the antivortex are sufficient for their identification. Second, the Cooper-pair density is significantly higher inside the V-Av molecule, since temperature may be far below T_c . Third, the magnetic field profile in the sample is sufficiently inhomogeneous, with pronounced amplitudes, benefiting from the size of the V-Av state and its stability for low values of κ . This is shown in Fig. 6 where the magnetic field profile in and nearby the sample is calculated for two values of κ for the second generation V-Av and for one value for the symmetry-induced V-Av (given in real units). For taken parameters, the magnetic field contrast inside the symmetry-induced V-Av molecule is of the order of 0.01 Oe, while that of the second generation V-Av can be above 10 Oe, thus three orders of magnitude larger.

Conclusion Using a square superconducting geometry with five holes, we found a second generation of the $L = 3$ vortex-antivortex (V-Av) state in a uniform field. This state is purely induced by pinning, and is NOT caused by the symmetry of the sample, contrary to the previously found V-Av molecules. This novel state is energetically favored in rather large mesoscopic samples, but it is never the ground state of the system. Con-

sequently, more elaborate techniques are needed for its stabilization in experiment, such as an abrupt increase of field (from negative to positive value), or an abrupt cooling of the symmetry-induced V-Av state. However, the very large $\Phi - T$ stability range of the second generation V-Av state, the very comprehensive size of the V-Av molecule, and the large variation in amplitudes of both superconducting order parameter and stray magnetic field inside the molecule (further enhanced for lower κ and temperature), all lead to facilitated experimental observation.

This work was supported by the Flemish Science Foundation (FWO-VI), the Interuniversity Attraction Poles (IAP), Programme-Belgian State-Belgian Science Policy, ESF-VORTEX program, and the ESF-AERO network. M.V.M. acknowledges support from the EU Marie Curie Intra- European program.

* Electronic address: francois.peeters@ua.ac.be

- [1] A.K. Geim, I.V. Grigorieva, S.V. Dubonos, J.G.S. Lok, J.C. Maan, A.E. Filippov, and F.M. Peeters, *Nature* (London) **390**, 259 (1997); A.K. Geim, S.V. Dubonos, I.V. Grigorieva, K.S. Novoselov, F.M. Peeters, and V.A. Schweigert, *Nature* (London) **407**, 55 (2000).
- [2] V.V. Moshchalkov, L. Gielen, C. Strunk, R. Jonckheere, X. Qiu, C. Van Haesendonck, and Y. Bruynseraede, *Nature* (London) **373**, 319 (1995).
- [3] V.A. Schweigert, F.M. Peeters, and P.S. Deo, *Phys. Rev. Lett.* **81**, 2783 (1998).
- [4] A. Kanda, B.J. Baelus, F.M. Peeters, K. Kadowaki, and Y. Ootuka, *Phys. Rev. Lett.* **93**, 257002 (2004).
- [5] L.F. Chibotaru, A. Ceulemans, V. Bruynndoncx, and V.V. Moshchalkov, *Nature* (London) **408**, 833 (2000).
- [6] V.R. Misko, V.M. Fomin, J.T. Devreese, and V.V. Moshchalkov, *Phys. Rev. Lett.* **90**, 147003 (2003).
- [7] A.S. Melnikov, I.M. Nefedov, D.A. Ryzhov, I.A. Shereshevskii, V.M. Vinokur, and P.P. Vysheslavtsev, *Phys. Rev. B* **65**, 140503(R) (2002).
- [8] J. Bonča and V.V. Kabanov, *Phys. Rev. B* **65**, 012509 (2001).
- [9] B.J. Baelus and F.M. Peeters, *Phys. Rev. B* **65**, 104515 (2002).
- [10] C. Carballera, V.V. Moshchalkov, L.F. Chibotaru, and A. Ceulemans, *Phys. Rev. Lett.* **95**, 237003 (2005).
- [11] R. Geurts, M.V. Milošević, and F.M. Peeters, *Phys. Rev. Lett.* **97**, 137002 (2006).
- [12] R. Geurts, M.V. Milošević, and F.M. Peeters, *Phys. Rev. B* **75**, 184511 (2007).
- [13] V.V. Khotkevych, M.V. Milošević, and S.J. Bending, *Rev. Sci. Instrum.* **79**, 123708 (2008).
- [14] M.V. Milošević, G.R. Berdiyrov, and F.M. Peeters, *Appl. Phys. Lett.* **91**, 212501 (2007).
- [15] G.R. Berdiyrov, B.J. Baelus, M.V. Milošević, and F. M. Peeters, *Phys. Rev. B* **68**, 174521 (2003).
- [16] J. Jurisson, and R. J. Oakes, *Phys. Lett.* **2** 187 (1962); E. Coskun, *Appl. Math. and Comp.* **106**, 31-49 (1999).
- [17] M.R. Connolly, M.V. Milošević, S.J. Bending, and T. Tamegai, *Phys. Rev. B* **78**, 132501 (2008).